We are IntechOpen, the world's leading publisher of Open Access books Built by scientists, for scientists

6,900
Open access books available

186,000
International authors and editors

200M
Downloads

154
Countries delivered to

Our authors are among the

TOP 1%
most cited scientists

12.2%
Contributors from top 500 universities

CLARIVATE ANALYTICS
BOOK CITATION INDEX
INDEXED

WEB OF SCIENCE™

Selection of our books indexed in the Book Citation Index
in Web of Science™ Core Collection (BKCI)

Interested in publishing with us?
Contact book.department@intechopen.com

Additive Manufacturing of Al Alloys and Aluminium Matrix Composites (AMCs)

Diego Manfredi, Flaviana Calignano,
Manickavasagam Krishnan, Riccardo Canali,
Elisa Paola Ambrosio, Sara Biamino, Daniele Ugues,
Matteo Pavese and Paolo Fino

Additional information is available at the end of the chapter

http://dx.doi.org/10.5772/58534

1. Introduction

In a product development context, the term Rapid Prototyping (RP) was widely used to describe technologies which created physical prototypes directly from digital data. The first methods for rapid prototyping became available in the late 1980s and were used to produce models and prototype parts. Users of RP technology have come to realize that this term is inadequate to describe the more recent applications of these technologies. The ASTM F-42 committee was recently formed to standardize Additive Manufacturing (AM) terminology and develop industry standards. According to their first standard, ASTM F2792-10, AM is defined as "*The process of joining materials to make objects from 3D model data, usually layer upon layer, as opposed to subtractive manufacturing technologies*". The basic principle of this technology is that a geometric model, initially generated using three-dimensional Computer Aided Design (3D CAD) system (e.g. CATIA, Pro/Engineer, SolidWorks), can be manufactured directly without the need of process planning [1].

There are many related terms used to describe AM and common synonyms include: additive fabrication, additive layer manufacturing, direct digital manufacturing, 3D printing and freeform fabrication. Within the last 20 years, AM has evolved from simple 3D printers used for rapid prototyping in non-structural resins to sophisticated rapid manufacturing systems that can be used to create functional parts in different engineering materials directly without the use of tooling. Most work to date has been conducted using polymer materials, but the development of AM processes such as Selective Laser Sintering/Melting, Electron Beam

Melting and Laser Engineered Net Shaping enabled to build parts by using metallic materials, metal matrix composites and ceramic materials. Additive manufactured parts are now utilized in aerospace, automotive, medical fields and also in consumer products and military [1-3].

Additive manufacturing or 3D printing is receiving unprecedented attention from the mainstream media, investment community, and national governments around the world. This attention reached a pinnacle when 3D printing was mentioned by United States President Barack Obama in his February 2013 State of the Union address. AM, just 25 years old and still a relatively small industry, has completed a transformation from obscurity to something that many can't stop talking about. In 2011, about 1600 articles were found. In 2012, they were 16000, a tenfold increase. Prototyping has been the technology's biggest application, thus the name rapid prototyping, and it remains a key category. The fastest-growing application, however, is in the actual manufacturing of parts for final products. In just 10 years, this important application has grown from almost nothing to more than 28% of the total global product and service revenues. The manufacturing of final parts, rather than prototyping, is where the manufacturing money is, and it is the most significant part of AM's future. Researchers and industry leaders in the European Union (EU) have identified AM as a key emerging technology. Teaming relationships have been formed between university, industry, and government entities within and across countries. The overall level of activity and infrastructure in the EU is greater to that of the U.S. in this key area. Several large cooperative projects have been funded, worth of millions of euros across Europe, among them AMAZE (Additive Manufacturing Aiming Towards Zero Waste & Efficient Production of High-Tech Metal Products) [4], RAPOLAC (Rapid Production of Large Aerospace Components) [5], Custom Fit (aiming at mass customized consumer and medical project manufacturing) [6], E-BREAK (Engine Breakthrough Components and Subsystems) [7], TiAlCharger (Titanium Aluminide Turbochargers-Improved Fuel Economy, Reduced Emissions) [8], and many others. Large aerospace companies, such as Boeing, GE Aviation, and Airbus, are hard at work qualifying AM processes and materials for flight. Boeing, for example, now has 200 different AM part numbers on 10 production platforms, including both military and commercial jets [9].

In 2013, NASA and Aerojet Rocketdyne have been testing rocket engine components made using additive manufacturing. At temperatures approaching 3300 °C, the AM rocket fuel injectors performed identically to conventionally manufactured parts. The series of tests demonstrated the ability to design, manufacture and test a critical rocket engine component using selective laser melting (SLM) manufacturing technology. This type of injector manufactured with traditional processes would take more than a year to make, but with these new processes it can be produced in less than four months, with a 70 percent reduction in cost [10]. The General Electric Aviation has used SLM to produce parts for its upcoming LEAP (Leading Edge Aviation Propulsion) family of turbofan engines, made in conjunction with France's Snecma.

AM technologies have the potential to change the paradigm for manufacturing, away from mass production in large factories with dedicated tooling and with high costs, to a world of mass customization and distributed manufacture. AM can be used anywhere in the product life cycle from pre-production prototypes to full scale production, as well as for tooling

applications or post production repair. AM processes are stimulating innovation in component design, enabling the manufacture of parts that cannot be made by traditional methods and are stimulating alternative business models and supply chain approaches. AM enables the manufacture of highly complex shapes with very few geometric limitations compared to traditional manufacturing processes.

This freedom of design, for example, has led to the technology being used to manufacture topologically optimized shapes with improved strength to weight ratios, a fundamental aspect in both aerospace and automotive design to reduce vehicle weight. For the bio-medical industry, AM is already leading to a revolution in customized medicine where dental implants, orthopedics, and hearing aids are manufactured to fit an individual's unique physiology.

However, despite many examples of growth and progress, many myths and misconceptions associated with the technology have developed:

• AM is a low-labor content "pushbutton" technology.

At the moment, a lot of work occurs before and after the actual production of the parts: in fact data needs to be prepared at the front end, which may require CAD expertise, the repair of the models, and optimization of support structures. Moreover, main building parameters, such as layer thickness, temperature, scan speed, and a number of other options may need to be adjusted for a particular part or type of material.

• AM is fast.

As the name implies, AM systems build parts by depositing, fusing, curing, or laminating consecutive layers of material. These layers are typically 0.025–0.250 mm in thickness, so parts often require thousands of layers. Therefore the preparation of large parts could take even several days.

• AM systems can produce anything.

Most of AM systems can successfully build shapes that cannot be fabricated easily or at all using conventional methods of manufacturing. However, AM processes also have limitations. One is minimum wall thickness. Another is the requirement for supports on down-facing surfaces, which can be difficult to remove. Material that is trapped in internal channels can also be difficult or impossible to remove, and the dimension of the internal channels determines the degree of difficulty in removing material.

• AM systems and materials are inexpensive.

Generally, industrial AM systems are more expensive than CNC machining centers, and starting materials are far more expensive (for example high quality powders, with controlled chemical composition, size and shape).

In any case, as AM continues to develop on multiple levels and in many directions, it will gain more momentum and respect as a method of manufacturing. Metal parts from some AM systems are already on par with their cast or wrought counterparts. As organizations qualify and certify these and other materials and processes, the industry will grow very large. 3D

printing is not competing with conventional manufacturing techniques, but is instead complementing and hybridizing with them to make new things possible.

2. Additive manufacturing processes for metals

It was less than 10 years ago that these systems began to gain traction commercially. Today, seven companies, all in Europe, offer systems based on powder bed fusion technology. Examples of powder bed fusion are direct metal laser sintering (DMLS) from EOS and selective laser melting (SLM) from Renishaw. The most popular metal systems use a laser to heat and melt fine particles in a powder bed. Parts obtained with these systems are impressive, especially the fine features and small internal channels that are possible.

Systems that instead use an electron beam as the energy source are much faster, but the surface finish and feature detail are not as impressive. In the case of some orthopedic implants, however, a rough surface is preferred. This, coupled with speed, is why many medical implant manufacturers have selected electron beam melting (EBM) systems from Arcam (Arcam is currently the only manufacturer to use electron beam energy in a powder bed). Many metal parts that are currently being made by AM can be cost prohibitive, difficult, or impossible to produce using conventional methods, such as casting or machining.

This gives AM an advantage, but only if the right types of parts are selected. Quality requirements play a role. Good feature detail and surface finish are possible and comparable to metal castings, but they do not match the surface quality of CNC machined parts. If a part can be produced conventionally at a reasonable cost and the volume is relatively high, it is often best to go that route at the present time. The metal AM systems are complemented by extensive CNC machining and other traditional processes.

Many types of metals are available on metal AM systems. Among the most popular for medical and aerospace applications is the titanium alloy Ti-6Al-4V. Other metals used are cobalt–chrome, stainless steels, tool steels, aluminium alloys such as AlSi10Mg, jewelry and dental gold alloys, nickel-based superalloys such as Inconel 625 and 718, and TiAl alloys. Aerospace-grade aluminium and other metals are in development. All of the unused metal powder can be recycled in the machines after sieving. Industry standards are becoming increasingly important as companies apply AM to the production of final products. In January 2012, ASTM International Committee F42 on Additive Manufacturing Technologies approved F2924-12 Standard Specification for Additive Manufacturing Titanium-6Aluminium-4Vanadium with Powder Bed Fusion. It is the first AM material standard by ASTM and it could give a boost to the additive manufacture of Ti-6Al-4V.

The technology classification agreed by the AM SIG (Special Interest Group) can be seen detailed in Table 1, which shows seven top level classifications for additive manufacturing technologies, below which there are a range of different material classifications, and discrete manufacturing technologies produced by a range of global companies.

Classification	Technology	Description	Materials	Developers (Country)
Binder Jetting	3D Printing Ink-jetting S-Print M-Print	Creates objects by depositing a binding agent to join powdered material	Metal, Polymer, Ceramic	ExOne (US) VoxelJet (Germany) 3D Systems (US)
Direct Energy Deposition	Direct Metal Deposition Laser Deposition Laser Consolidation Electron Beam Direct Melting	Builds parts by using focused thermal energy to fuse materials as they are deposited on a substrate	Metal: powder and wire	DM3D (US) NRC-IMI (Canada) Irepa Laser (France) Trumpf (Germany) Sciaky (US)
Material Extrusion	Fused Deposition Modeling	Creates objects by dispensing material through a nozzle to build layers	Polymer	Stratasys (US) Delta micro Factory (China) 3D Systems (US)
Material Jetting	Polyject Ink-jetting Thermojet	Builds parts by depositing small droplets of build material, which are then cured by exposure to light	Photopolymer, Wax	Stratasys (US) LUXeXcel (Netherlands) 3D Systems (US)
Powder Bed Fusion	Direct Metal Laser Sintering Selective Laser Melting Electron Beam Melting Selection Laser Sintering	Creates objects by using thermal energy to fuse regions of a powder bed	Metal, Polymer, Ceramic	EOS (Germany) Renishaw (UK) Phenix Systems (France) Matsuura Machinery (Japan) ARCAM (Sweden) 3D Systems (US)
Sheet Lamination	Ultrasonic Consolidation Laminated Object Manufacture	Builds parts by trimming sheets of material and binding them together in layers	Hybrids, Metallic, Ceramic	Fabrisonic (US) CAM-LEM (US)
VAT Photopolymerisation	Stereolithography Digital Light Processing	Builds parts by using light to selectively cure layers of material in a vat of photopolymer	Photopolymer, Ceramic	3D Systems (US) EnvisionTEC (Germany) DWS Srl (Italy) Lithoz (Austria)

Table 1. Classification of additive manufacturing processes defined by the AM SIG – adapted from ASTM AM classifications (2012) [11].

3. Direct metal laser sintering — DMLS

Direct Metal Laser Sintering (DMLS), a trademark of EOS GmbH (Germany), is an Additive Manufacturing (AM) technology that creates parts in a layer-by-layer fashion directly from

computer-aided design by selectively fusing and consolidating thin layers of powders with a scanning laser beam. DMLS is a net-shape process, producing parts with high accuracy and detail resolution, good surface quality and excellent mechanical properties. As mentioned before, it has many benefits over traditional techniques and its application for manufacturing three dimensional objects represents one of the promising directions to solve challenging industrial problems. Moreover, since the components are built layer by layer, it is possible to design internal features and passages that could not be cast or otherwise machined. Complex geometries and assemblies with multiple components can be simplified to fewer parts with a more cost effective assembly. DMLS does not require special tooling like castings, so it is convenient for short production runs. Applications using this technology include direct parts for a variety of industries including automotive and other industries that use complex parts of small to medium size. For instance, concerning space applications, when the "buy to fly ratio" of a structure is below about 30%, meaning that more than 70% is machined away, additive manufacturing technologies become an alternative to conventional machining for complex metallic parts. And when direct manufacturing allows to produce in one shot spacecraft structures resulting from complex assemblies, then the offered possibilities are really huge. DMLS has also already been used to fabricate lightweight structures, similar to cellular structures. Inspiring to natural systems, a variety of synthetic cellular solids could be made including stochastic foams, consolidated powders, hollow sphere structures, honeycombs, textile laminates and lattice block or miniature truss structures. The cellular metal structures have been used in various industrial applications such as heat exchangers, in automotive and aerospace industries, thanks to their valuable characteristics as low density, high strength, good energy absorption and good thermal properties. Virtually any material can be produced by additive manufacturing, most of those by DMLS, with the exception of some intermetallic and high temperature alloys.

One of the most interesting types of these materials are aluminium alloys. It is rather easy to produce alloys with compositions suitable for casting, since they will melt easily, but recently wrought alloys have also been fabricated by this technique, and new ones are being studied. The microstructure of these alloys is peculiar, since the very fast cooling occurring after the melting induced by laser provides an ultra-fine microstructure and this is responsible for a significant increase of the mechanical properties that can be obtained with conventional casting processes followed by heat treatments. It is also possible, to increase specific properties of the alloy, to produce aluminium matrix composites (AMC). These could have applications in high-demanding components, for instance in automotive and aerospace industries, where it is necessary to improve stiffness, hardness and high temperature properties. Ceramic discontinuous reinforcements are the most suitable reinforcement that can be envisaged.

4. DMLS process

Initially, all contour of the layer structure is exposed with a selected laser power and contour speed. As the diameter of the melted zone is usually larger than the laser diameter, it is necessary to compensate the dimensional error and the laser beam must be shifted by half the

width from the contour to the inside, to make sure that the contour of the later part will correspond exactly to the original CAD data. This correction of the position is called Beam Offset (BO) [12]. The BO value is again defined with respect to the edge of the boundary (Figure 1), and if this value is higher or less than the correct value, the particles of the irradiated region may be not melted or over-melted. During hatching, the laser beam moves line after line several times to assure that the melting process can unroll completely. The distance between the lines is called hatching distance (h_d) and is set about one quarter of the laser beam.

Another important parameter that can lead to a distorted part or a process interruption is the layer thickness. If the value is too high, no optimal adhesion between the single layers can be realized because the melting depth is not high enough. Furthermore, mechanical tension can be generated through this layer which can lead to detachment of the layer below. If the selected value is too small, a tearing-off of a structure can happen during the recoating process, since the melted particles get struck between it and recoater blade [12].
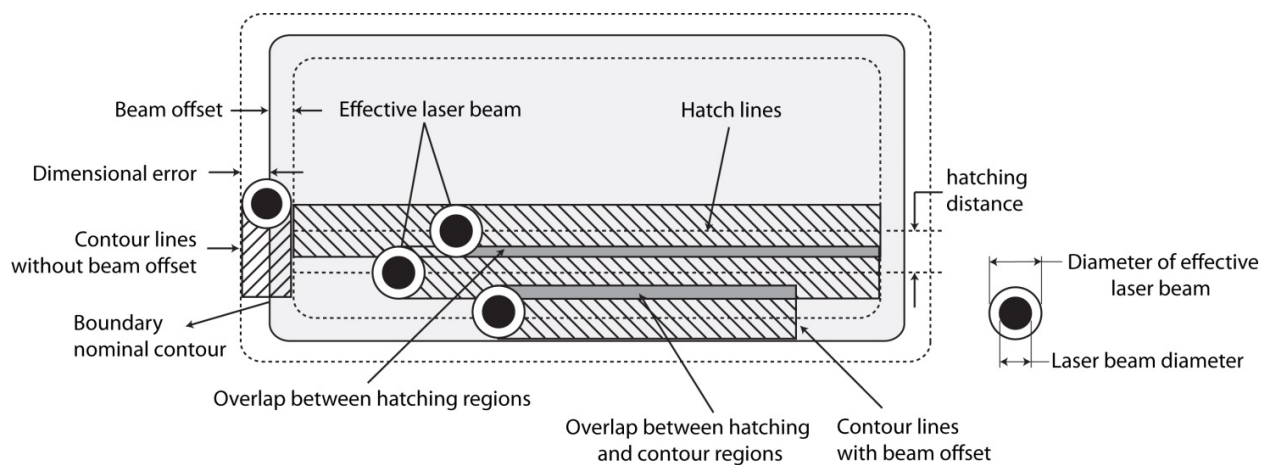

Figure 1. Exposure strategies.

5. DMLS scanning strategy

Many scanning options are provided in commercial SLM machines which include skywriting and hatch pattern along x, y, both in xy and alternating in xy for different requirements. DMLS EOS machine has up-skin and down-skin options to improve mechanical properties by allowing user to assign different process parameters at adjoining layers. Subsequent paragraphs illustrate salient features of scanning strategies available with DMLS process.

5.1. Skywriting

During scanning a certain time is needed to accelerate the mirrors to the desired speed. This is due to inertia of mirrors used for scanning. During this time laser beam cover some distance in which speed is not constant hence more energy is applied at the edges of the part than the

inside of the part. To avoid this situation and to keep acceleration and retardation phase out of the layer geometry, skywriting option is provided in DMLS machines. If skywriting option is selected, then the mirror is accelerated already before the start of the part so that it has reached the desired speed before the beginning of exposure. Laser is switched on at the start of the part. Similarly retardation phase begins at the part end where the laser is switched off as shown in Figure 2.
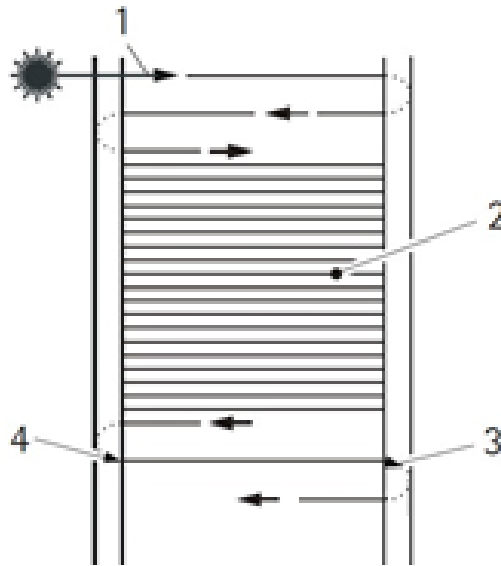

Figure 2. The exposure vector is shown by a solid line (1). The dashed line presents the skywriting. In this area the laser beam is run with a laser power of 0 W (3). With the beginning of the part (4), the laser power switched on with a sized value and the laser beam is running with a constant velocity.

5.2. Hatch pattern

Four choices for hatch pattern selection are generally available, i.e., along x, along y, both in xy or alternating in xy as shown in Figure 3. Scanning can be done either along x or along y (Figure 3a and 3b). If both in x and y options are selected than there will be double exposure on the layer, once along x and then along y (Figure 3c). In alternating in xy choice, direction of scanning is changed for alternating layers (Figure 3d). Figure 3e shows the direction of scanning rotated of 67° between consecutive layers. This is default value of the hatch pattern in DMLS EOS machine.
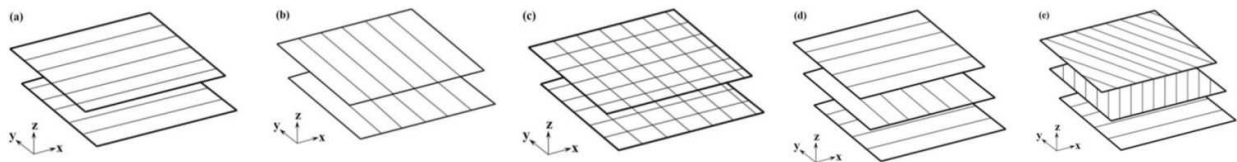

Figure 3. Different hatch patterns or scanning strategies.

5.3. Up-skin and down-skin

The layer above which there is no area to be exposed, is termed up-skin, and is built in three layers. Similarly the layer below which there is no exposed area is called down-skin, and is built in two layers. The rest of the part is termed core or in-skin, and is shown in Figure 4. Commercial machine software calculates up-skin, down-skin and core areas and different parameters can be assigned for these areas. Some overlapping area between core and up-down-skin area can also be assigned for improved joining among these zones.
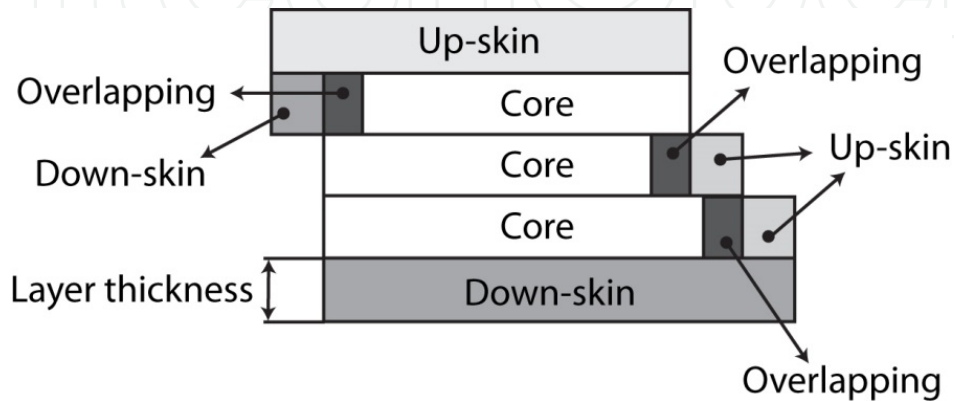

Figure 4. Up-skin, down-skin and core regions.

6. Materials processed by DMLS

Table 2 condenses a list of metal-based materials processed by SLM/DMLS as available in the literature.

Some of the main common features for different materials processed by SLM are summarized hereafter.

Microstructure: small grains, non-equilibrium phases and new chemical compounds are formed during SLM of metal powders [28,40].

Mechanical properties: due to the formation of very fine grains and non-equilibrium structures, the SLM parts could exhibit better mechanical properties (yield strength, ultimate tensile strength and ductility) than the wrought products [28]. Yasa et al. [20] have studied the Charpy impact test of TiAl6V4, A316L stainless steel and maraging steel parts produced by SLM. Spierings et al. [41] have investigated the influence of three different size distribution of 316L stainless steel powder on mechanical properties and surface quality. Their research concluded that powder with smaller size particle distribution could be easily melted and yields high density, high mechanical strength and productivity.

Anisotropy: the parts are produced by stacking layers in SLM, due to this reason the parts have some anisotropy in a particular direction. Buchbinder et al. [42] have investigated the fatigue

Family	Material	References
Metals and alloys	Steel	hot-work steel [13]
		stainless steel 316L [14-17]
		martensitic steel [18]
		tool steel [15-19]
		maraging steel [20]
	Titanium	Ti6Al4V [21-24]
		Ti6Al7Nb [25]
	Nickel based alloy	Inconel 718 [26]
		Inconel 625 [27]
	Copper	copper [28-29]
	Gold	Gold [30]
	Aluminium	A6061 [31]
		AlSi12 and AlSi12Mg [32,33]
		AlSi10Mg [34-37]
Composites	MMC	Fe-graphite, Ti- graphite/diamond, Ti-SiC, AlSi-SiC, AlMg-SiC, Co-WC, Fe-SiC and Cu, Ni, Ti, C, Cu-TiC and Cu, Ni, Ti, B_4C, Cu-TiB$_2$ [38]
		Al4.5Cu3Mg-SiC [39]
	CMC	ZrO2, Y_2O_3, Al, Al_2O_3 and TiO_2,Al,C TiC/Al_2O_3 [38]

Table 2. Examples of materials used in SLM/DMLS.

testing of AlSi10Mg parts produced by SLM. Their investigation concluded that sample produced in x plane exhibited higher fatigue resistance than samples produced in other orientations. Yadroitsev et al. [27] have studied the mechanical properties of SLM parts. They found that Young's modulus of Inconel 625 parts produced in xy plane are 1.5 greater than that of parts produced in z direction. Qiu et al. [43] studied the microstructure and tensile properties of Ti6Al4V parts produced by SLM in two different orientations. They found that Ti6Al4V parts show high tensile strength, but the Ti6Al4V samples oriented along z axis showed higher ductility than that of sample oriented in xy plane. This anisotropy was caused by the orientation of the columnar grains with respect to the tensile test direction. Thijs et al. [44] studied about SLM of tantalum parts. Their study revealed that grains were oriented in <111> direction, because of partial re-melting of the previous layer, competitive growth mechanism and specific global direction of heat flow during SLM of tantalum. This texture formation had a large influence on yield strength during compression test of tantalum parts.

Residual stresses: these are induced in the SLM parts due to the complexity in melting behavior of layers. Re-melting and solidifying of previously melted layers can cause stress field to exceed the yield strength of the material, causing distortion of the part. Studies show that island scan

strategy could reduce the residual stress of SLM parts [45]. Shiomi et al. [46] measured residual stress of chromium molybdenum steel parts produced by SLM. They found that: performing stress relieving treatment of build platform along with parts at about 700 °C for one hour, decreased residual stress by 70%, re-scanning of each layer reduced the residual stresses by 55% and heating of build platform to 160 °C reduced the residual stresses by 40%. Mercelis and Kruth have used crack compliance method and XRD to measure residual stress of 316L stainless steel parts produced by SLM. Zaeh and Branner [47] have carried out Finite Element Analysis to evaluate residual stress of steels processed by SLM and they also measured residual stress by using neutron diffraction.

Surface Roughness: the surface roughness of the SLM parts is higher than that of conventionally produced parts. Vertical faces of the part have lower surface roughness than that of curved or inclined or top faces. To improve the surface finish of the SLM parts, secondary operations like shot peening, machining or abrasive jet machining are carried out. Kruth et al. [48] showed that the surface quality of Stainless steel 316L and Ti6Al4V parts could also be improved in SLM by using Selective Laser Erosion (SLE) and re-melting. Calignano et al. [12] have improved the roughness of AlSi10Mg parts produced by DMLS process.

7. Case study — AlSi10Mg parts by DMLS

7.1. Experimental equipment

Aluminium alloy samples were produced by DMLS with an EOSINT M270 Xtended version. In this machine a powerful Yb (Ytterbium) fiber laser system in an argon atmosphere is used to melt powders with a continuous power up to 200 W and a spot size of 100 μm. The aluminium powder alloy used in this study is a gas atomized one produced by EOS Gmbh (Germany), and its nominal composition is reported in Table 3.

Element	Si	Fe	Cu	Mn	Mg	Zn	Ti	Al
Weight %	9-11	≤0.55	≤0.05	≤0.45	0.2-0.45	≤0.1	≤0.15	remainder

Table 3. Nominal composition of EOS AlSi10Mg alloy powder in accordance with standard DIN EN 1706:2010-06.

This alloy is similar to an A360.2 alloy [49]: thanks to its near eutectic composition in the Al-Si phase diagram it is often used in casting, having a melting temperature around 570 °C. This alloy offers good strength and hardness and is therefore used for parts with thin walls and complex geometry subjected to high loads, as in the aerospace and automotive industries.

Table 4 shows the default values assigned to up-skin, down-skin and core for the scan speed, laser power and hatching distance parameters in producing the Al alloy specimens.

Samples of rectangular shape and 50 × 10 × 3 mm size were produced to analyze the density, hardness and Young's Modulus. Considering tensile tests, specimens were built according to

Parameters	Core	Up-skin	Down-skin	Contour
Scan speed (mm/s)	800	1000	900	900
Laser power (W)	195	195	190	80
Hatching distance (mm)	0.17	0.2	0.1	

Table 4. Default values of scan speed, laser power and hatching distance for EOS M270 Xtended.

the standard ASTM E8M. For the analysis on the surface roughness, the three input or control factors chosen for up-skin were scan speed, laser power and hatching distance (Table 5). The surface finish of the samples was then analyzed though a 3D scanner ATOS Compact Scan 2M (GOM GmbH) and a MarSurf M 300C (Mahr GmbH) mobile roughness measuring instrument before and after post-processing. To compare the different DMLS samples, the average value of the ordinates from centerline, defined as Ra, was used. It is theoretically derived as the arithmetic average value of departure of the profile from the mean line along a sampling length. The shot-peening process was performed with glass microspheres using a sand-blasting machine, SD9 Northblast, in order to improve their surface finishing. The samples, before and after shot peening, were also characterized by a Field Emission Scanning Electron Microscope (FESEM) Zeiss SupraTM 40.

Variable Parameters	Values
Scan speed (mm/s)	800, 850, 900, 950, 1000, 1250
Laser power (W)	120, 155, 190
Hatching distance (mm)	0.10, 0.15, 0.20
Fixed Parameters	**Values**
Layer thickness (µm)	30
Spot size (mm)	0.1

Table 5. Process parameters values for the up-skin.

7.2. Powder analysis

The AlSi10Mg powder was gas atomized and supplied by EOS GmbH. A preliminary observation was made to investigate the morphology of the AlSi10Mg powder particles by using the FESEM described above.

The spherical morphology and smooth surface of the powder particles result in a good flowability and homogeneous layer distribution [36]. Figure 5 shows the FESEM micrograph of AlSi10Mg powder in as received condition. The size of AlSi10Mg powder ranges from 1 to 35 µm with an average size around 23 µm. Bigger clusters of dimension larger than 40 µm were also observed. Thus the powder was sieved to separate the agglomerated powder particles each time before producing the final part in DMLS process.

Material	Orientation	Yield Strength [MPa]	Ultimate Tensile Strength [MPa]	Elongation at break [%]
AlSi10Mg after DMLS	xy-plane	240 ± 8	330 ± 4	6.2 ± 0.4
	z axis	230 ± 5	328 ± 4	4.1 ± 0.3
A360.0 F *	–	170	317	5

Table 7. Mean values of tensile properties of aluminium alloy DMLS specimens produced according the standard ASTM E8M, compared to a similar alloy in as-fabricated conditions [*].
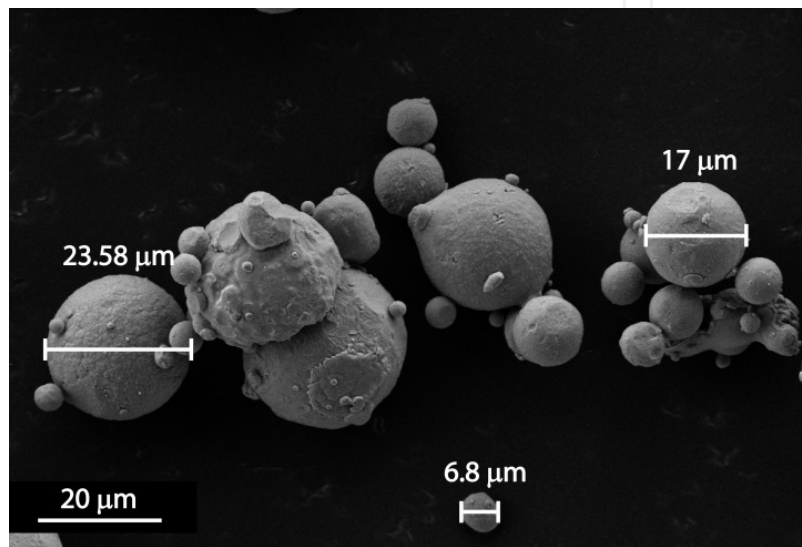

Figure 5. FESEM observation of AlSi10Mg powder.

In Table 6 are summarized the mean values for density, Young's modulus and Vickers Hardness. Moreover, considering for the AlSiMg alloy a theoretical density of 2.68 g/cm^3 [49], the percentage of the residual porosity can be calculated.

Density (g/cm^3)	Residual Porosity (%)	Hardness (HV)	Young's Modulus E (GPa)
2.66	0.8	105 ± 5	73 ± 1

Table 6. Density, Hardness and Young's Modulus of aluminium alloy DMLS specimens.

Considering tensile tests, the results are summarized in Table 7. Variations were not found among performances of samples with different orientations on the powder deposition plane, while there are some differences with the values obtained along the direction perpendicular to it, as already discussed in a previous paragraph. In fact, as the name implies, the parts are produced by stacking layers in SLM, due to this reason the parts have some anisotropy in the so called "building direction", or z axis.

The AlSi10Mg DMLS specimen microstructure was analyzed by optical microscopy (Leica DMI 5000 M optical microscope) and by FESEM. Top and a lateral surfaces of the specimens were polished by using SiC abrasive papers of different grits and then by using 6 μm, 3 μm and 1 μm diamond pastes respectively. Then they were etched with Weck's reagent or HF in water to highlight the scanning tracks or melt pools. The dimensions of the melt pools (width and depth) depend on the laser power and hatching distance employed, and also on the scanning strategy (Figure 3).

Figure 6 shows the optical microscopy images of AlSi10Mg specimen. Hauser et al. have reported that the cross-section of the single tracks formed in SLM process were either crescent shape or elliptical section [50]. From the optical micrograph of the AlSi10Mg sample polished in the lateral surface (z direction), a typical crescent shape structure can be noticed, if the scan track or melt pool is oriented perpendicular to the polished surface (Figure 6, on the left). Some elongated scan tracks are also observed, when the scan track is aligned at an angle with respect to the polished surface. This is due to the scanning strategy of the laser beam adopted (see Figure 3e). Figure 6 shows also the optical microscopy image of AlSi10Mg specimen polished in xy plane. The cross section of scan tracks of different layers and the overlapping of scan tracks can be observed.
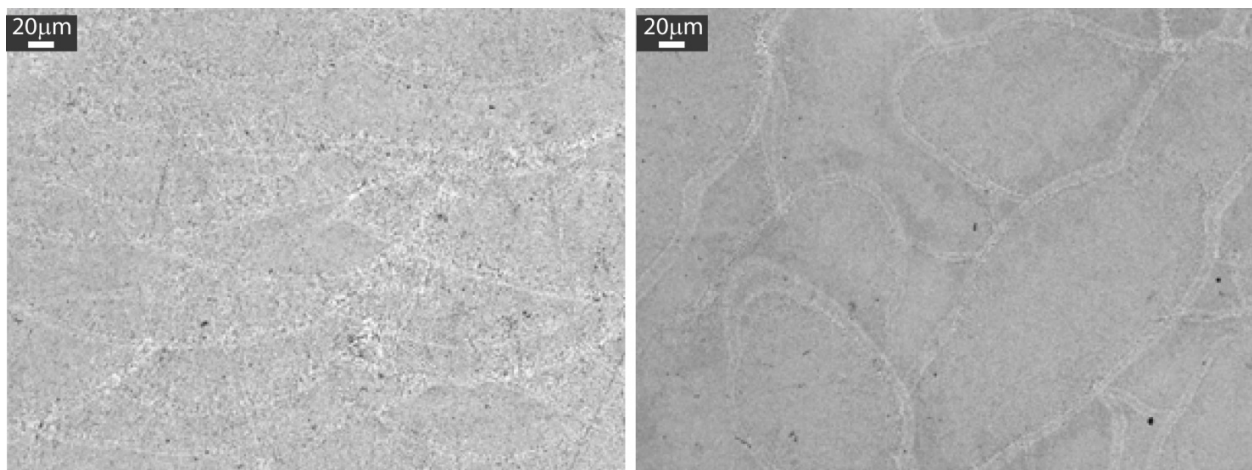

Figure 6. Microstructure of AlSi10Mg along *Z* direction (on the left) and along *XY* plane (on the right) after etching with HF in water reagent.

The geometry of the scan tracks was not clear with the default scanning strategy, because the scan lines are always rotated by 67° with respect to the scan lines of previous layer (see Figure 3e). In order to observe the geometry of the scan tracks, a specimen was produced by orienting the scan lines along *x* axis. Figure 7 (a) and (b) show the microstructure of AlSi10Mg sample produced by orienting scan tracks only along *x* axis (see Figure 3b).

It can be observed that the shape of scan tracks is crescent or elliptical. However, this specimen had a higher porosity with respect to the ones obtained with the default scanning strategy. Therefore, the default scanning strategy with 67° is generally chosen to produce AlSi10Mg samples for the measurement of mechanical properties.
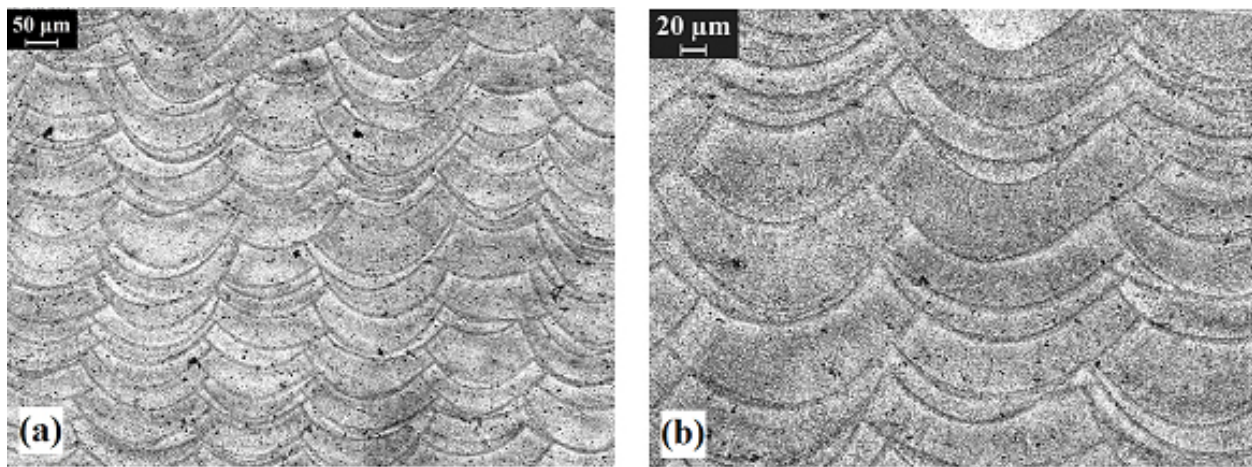
Figure 7. Optical micrographs of AlSi10Mg specimen produced by orienting scan tracks along x axis, after etching with Weck's reagent [51].

To appreciate the small grain size, the section along the build direction was observed by FESEM, focusing on a region between adjacent melt pools, as shown in Figure 8. After etching with HF and going at higher magnification, it can be seen that the melt pool contour region is characterized by a fine cellular-dendritic structure made by agglomerates of grains with mean diameters of a hundred of nanometers or less [37]. It was found that these agglomerates are different in length, thickness and aspect ratio, probably due to the different thermal heat fluxes during each scanning track.
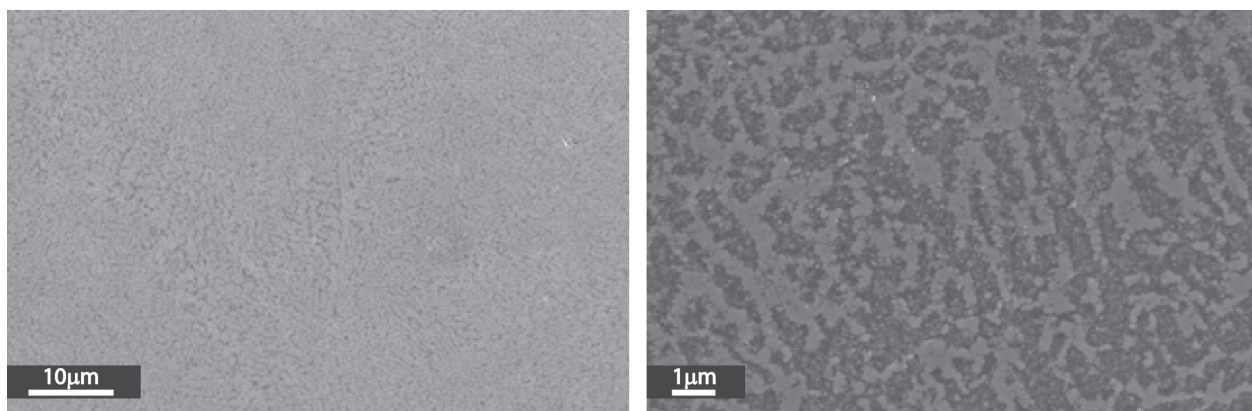

Figure 8. FESEM observations of AlSi10Mg specimen before etching (on the left), and after etching with HF (on the right) at higher magnification.

Also, fracture surfaces after tensile tests were investigated by FESEM, as reported in Figure 9. As can be seen, the surface is covered by very fine dimples, clearly visible only at high magnification. On the left image there can also be observed two little concave zones probably related to two spherical particles not completely melted. At higher magnification is possible to appreciate the very fine dimension of the microstructure, with presence of particles of tens of nanometers.
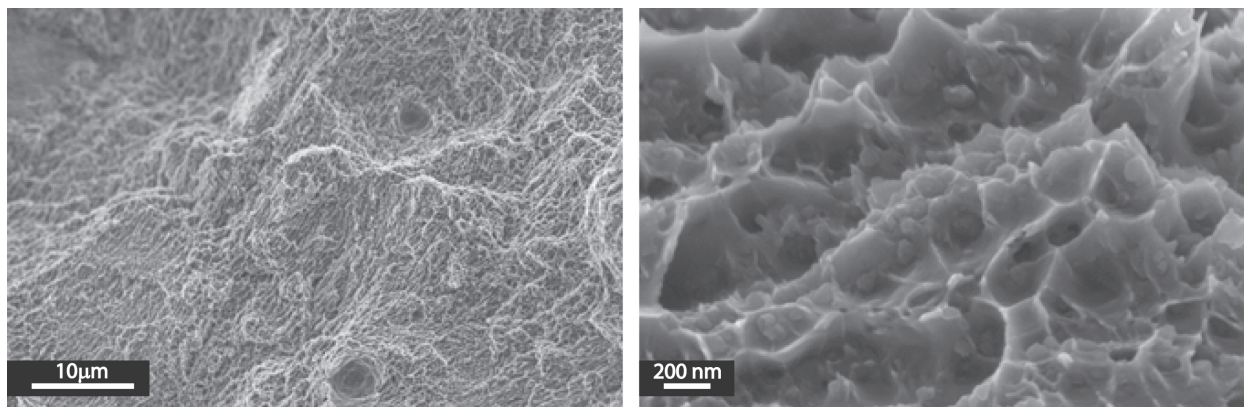
Figure 9. FESEM images of an aluminium alloy DMLS fracture surface covered by sub-micrometric voids and dimples with a nanometric size.

7.3. Effect of heat treatments

Due to the high thermal gradients, DMLS process fabricates parts with high residual thermal stresses. In order to avoid the bending of the AlSiMg parts fabricated, before removing them from the building platform, it is fundamental to perform an annealing for 2 h at 300 °C. Annealing offers very good dimensional and physical stability of the parts. It also provides the lowest level of residual stresses. The cooling is done in furnace or in the still air.

Apart from this, it is not common to perform a post heat treatment such as for conventional casting alloys. However, it is well known that mechanical properties of aluminium alloys are affected by heat treatments. Hence, the influence of heat treatments on hardness and tensile properties of AlSi10Mg parts produced by DMLS process was also investigated. In particular, annealing (T2), T4 and T6 heat treatments were carried out on fifteen AlSi10Mg samples for mechanical testing instead of stress relieving [51]. After the heat treatment, the hardness and tensile properties of these specimens were evaluated.

The first specimens were subjected to annealing treatment at 530 °C for 5 hours and cooled in the furnace. The second samples were obtained in T4 heat treatment: solution heat treated at the temperature of 530 °C for 5 hours and then quenched in water, followed by a room temperature ageing of at least two weeks. Finally the last samples were subjected to a T6 heat treatment cycle [49]. In this case, the AlSi10Mg specimens were solution heat treated at the temperature of 530 °C for 5 hours, then quenched in water and artificially aged at 160 °C for 12 hours.

The specimens were polished and the micro hardness was measured by using a Leitz instrument. The indentation load used was 50 g and duration of the indentation was 30 seconds. The results are illustrated in Table 8. The hardness after the T6 heat treatment is 13% higher than the mean value of the laser sintered AlSi10Mg samples just after the stress relieving treatment (105 HV, Table 6). Considering the T4 heat treatment, it reduced hardness by 15 % compared to AlSi10Mg sample without heat treatment, while with annealing the mean hardness was reduced by 58 %.

Type of heat treatment	Hardness (HV)	
	mean	S.D.
Annealing	46	3
T4	89	7
T6	119	6

Table 8. Effect of heat treatment on hardness of AlSi10Mg samples.

Tensile tests were also performed on AlSi10Mg after heat treatments. Again the specimens were produced according to ASTM E8M. The specimens were produced in the xy plane orientation by using DMLS process. Post processing operations such as shot peening or machining was not carried out on these specimens after heat treatments. The tensile tests of heat treated AlSi10Mg specimens were carried out by using EasyDur 3MZ-5000.

The results of the tensile tests are summarized in Table 9 [51].

Type of heat treatment	Rp0.2 (MPa)		UTS (MPa)		%A	
	mean	S.D	Mean	S.D	Mean	S.D
Annealing	72	7	113	3	12.6	0.9
T4	131	9	227	4	6.9	0.8
T6	245	8	278	2	3.6	0.8

Table 9. Tensile properties of AlSi10Mg specimens after heat treatments [51].

It can be concluded that all the heat treatments reduced the tensile properties of AlSi10Mg specimens (see also Table 7). Annealing reduced the ultimate tensile strength by 66 %, when comparing to the tensile strength of AlSi10Mg specimens in "as built" condition (just after DMLS, without shot peening). However, the elongation was improved by 103%, as expected. The tensile strength of the AlSi10Mg specimens after T4 treatment was reduced by 31% and ductility was improved by 11%, respectively. The ultimate tensile strength and elongation of the AlSi10Mg samples after T6 heat treatment were decreased by 16% and 42%, respectively. The only improvement observed after heat treatment is a slight improvement in yield strength, from 240 to 245 MPa, for the T6 samples with respect to the "as built" condition.

Stress-strain curves obtained from tensile tests of specimens after different heat treatment conditions are compared in Figure 10.

FESEM analysis of the fracture surfaces after different heat treatments were also performed, and the micrographs are shown in Figure 11. It can be seen that the dimensions of the dimples of fracture surface after each heat treatment considered are greater than the dimples of the corresponding fracture surface just after a stress relieving treatment. The total energy of the fracture is related to the size of the dimples [52]. Brandl et al. have reported that the SLM
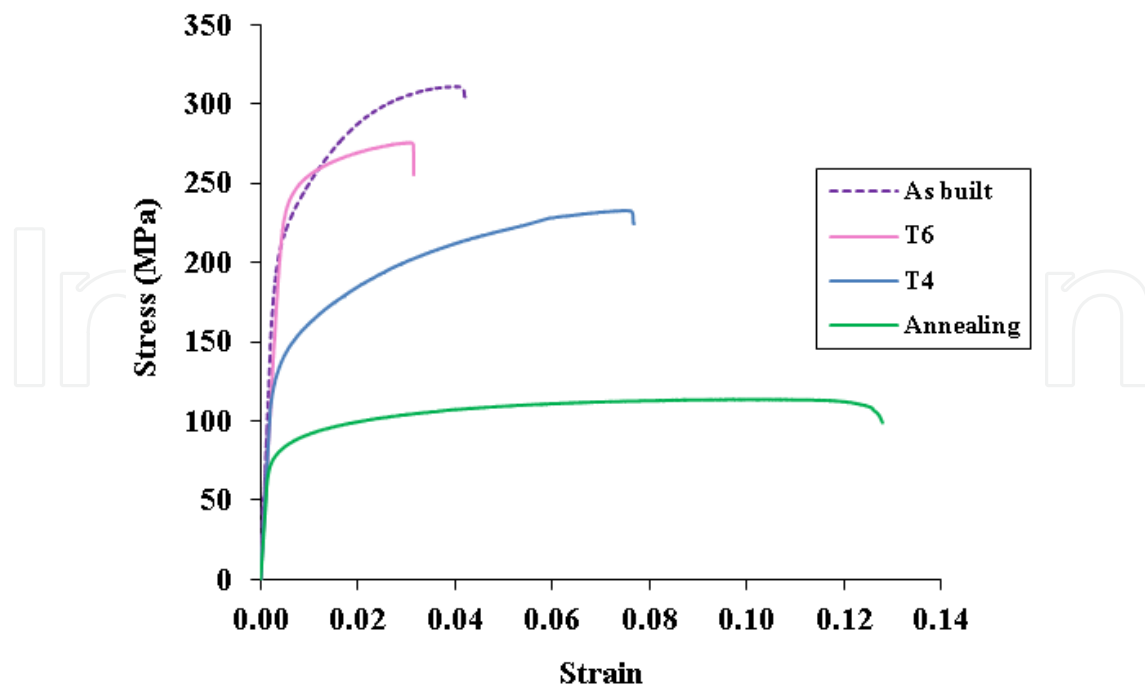
Figure 10. Stress vs strain curves of AlSi10Mg specimens in "as built" condition and after heat treatments [51].

processing of AlSi10Mg by maintaining the build platform at 300 °C and T6 heat treatment after SLM increase the fatigue resistance. This is due to homogenizing of microstructure after T6 heat treatment [53].

7.4. DMLS samples surface morphology

Due to its versatility of materials and shapes, the main advantage of DMLS is to produce metal complex-shaped components in one step, but it also has drawbacks that require careful process control: the high temperature gradients and densification ratio during the process yield high internal stresses or part distortion; the risk of balling and dross formation in the melt pool may result in bad surface roughness (from 8 to 20 μm without any post-treatment) [54-55]. The surface finish of a part, defined as the irregularities of any material resulting from machining operations, is critical in many applications, for example those requiring a surface roughness of 0.8 μm or better to avoid premature failure from surface initiated cracking [56]. There is no standard method to enhance the surface quality due to the complex nature of the process and to the different properties of the materials used [54,57]. Laser parameters like laser beam power, spot size and process parameters like scanning speed, hatching distance and layer thickness have a great influence on the quality of the laser sintered samples. The effect of some process parameters on AlSi10Mg parts produced by DMLS was studied through statistically designed experiments based on an L_{18} orthogonal array of Taguchi design [12]. Scan speed was found to have the greatest influence on the surface roughness. The Taguchi method uses *S/N* ratio to measure the variations of the experimental design. The equation of *smaller-the-better* was selected for the calculation of *S/N* ratio since it yields the lowest values of surface rough-
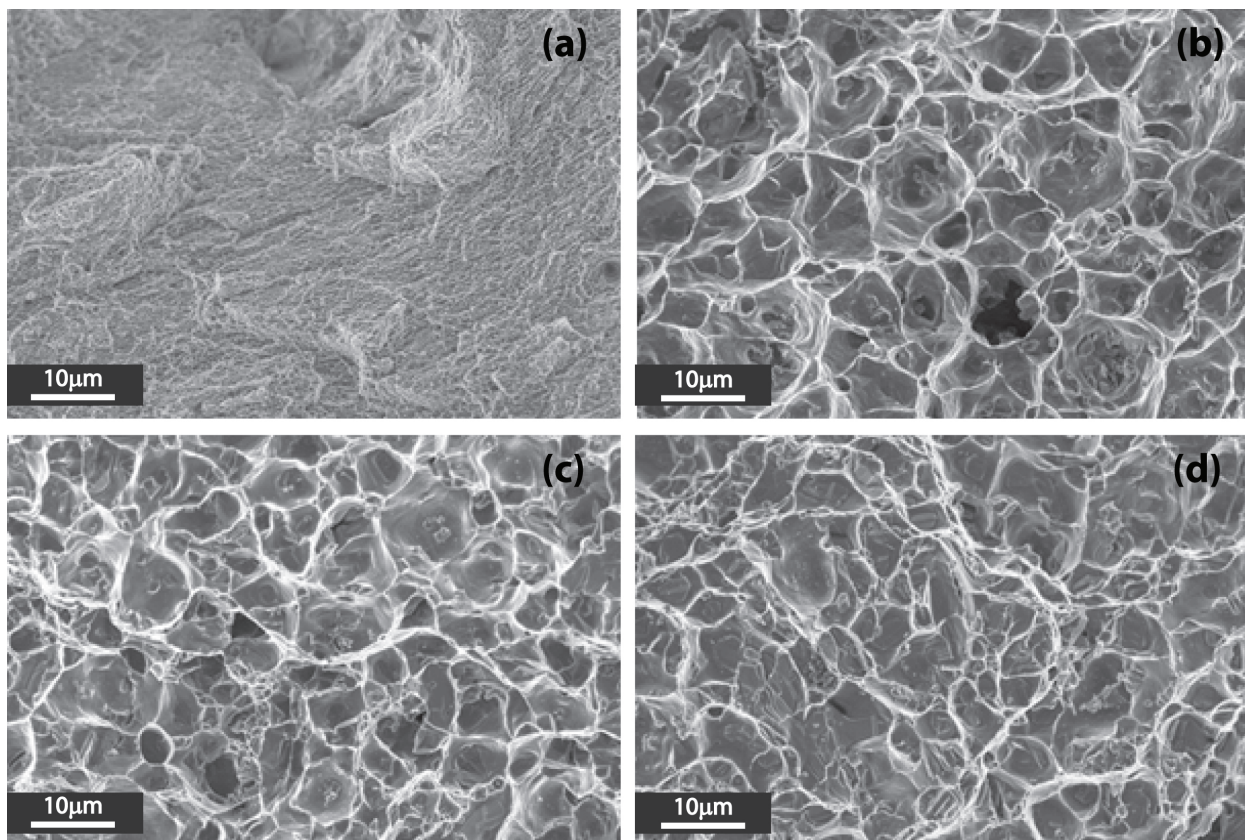
Figure 11. FESEM images at the same magnification of fracture surfaces after DMLS and a stress relieving treatment (a), after an annealing treatment – T2 (b), a T4 treatment (c) and a T6 treatment (d)

ness. It was found that S/N ratio is minimized when the scan speed is 900 mm/s, the laser power is 120 W, and the hatching distance is 0.10 mm.

The process of shot-peening involves a mechanical surface treatment whereby small balls impinge on the surface of the component. The repeated impacts not only induce compressive residual stress but also refine the microstructure at the surface and sub-surface region [58,59]. The near surface compressive residual stress field reduces the effective applied stresses of the component during application, which results in delayed crack initiation and retarded early crack propagation. It is important that shot-peening method is optimized to improve the depth of favorable compressive residual stress fields while minimizing surface roughening [59,60].

Figure 12 shows the surface roughness of a sample after the DMLS process (R_a=23.08 μm, R_z=152.92 μm) and then after the shot-peening post processing treatment (R_a=3.35 μm, R_z=31.81 μm). Thanks to the use of a 3D scanner is possible to analyze the entire surface (Figure 12a and 12d) and define the deviation of these from the best-fit 3D plane. The deviation of the sample before and after shot-peening is of 0.17 mm and 0.07 mm respectively (Figure 12b and 12e). Surface topography is classically characterized by surface profiles obtained via electronic contact profilometry (Figure 12 c and 12f).
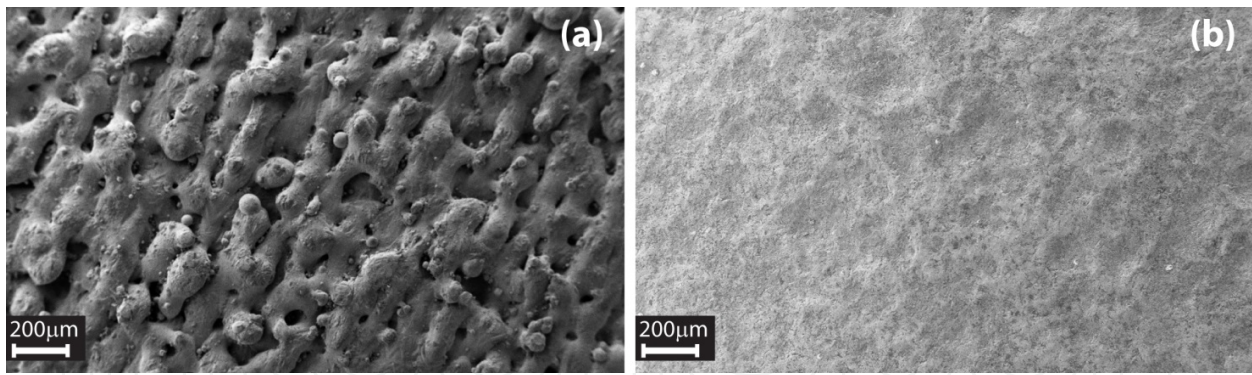
Figure 13. FESEM images of surface roughness of (a) sample with R_a=23 μm and (b) sample after shot peening at 8 bar.
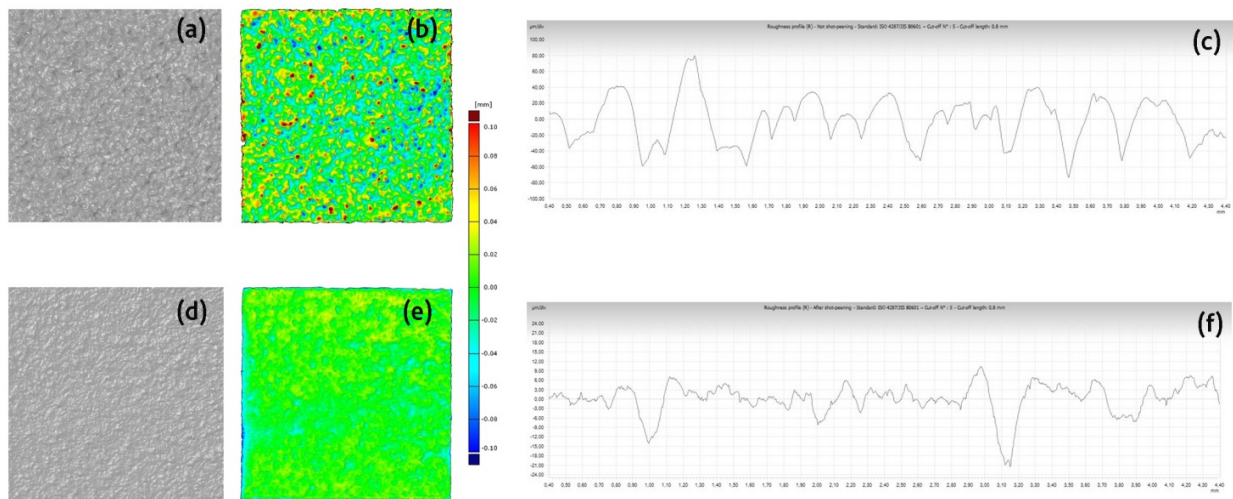

Figure 12. (a) 3D scan surface roughness of a DMLS AlSiMg sample before and (d) after shot-peening. (b) Deviation color maps respect to best fit plane before and (e) after shot-peening. (c) Roughness profile of the sample before and (f) after shot-peening.

Different roughness parameters are then extracted from the acquired surface profile. Among all the parameters for quantifying surface roughness based on tactile profile sections, R_a, the arithmetical mean deviation of the assessed profile, is by far the most extensive and most used parameter. It possible to see that shot peening with glass beads makes to significantly reduce the surface roughness. Different values of shot peening pressure were analyzed. The best results were obtained using a pressure of 8 bar: the surface roughness was reduced by up to 85%. These considerations on laser sintering parameters and the shot peening effect were confirmed by FESEM observations (Figure 13): the images give evidence of the improvement in surface roughness.

7.5. Lightweight metal structures by DMLS

One of the main interesting applications of additive manufacturing is for fabrication of customized, lightweight material structures, like periodic cellular lattice structures [61]. The

word "cell" derives from the Latin word *cella* meaning a small compartment or enclosed space [62]. When nature constructs things, it is often done from many cells (cellula). Wood and cancellous bone are good examples of this: they are stiff, lightweight and multifunctional. From these natural inspirations a variety of synthetic cellular solids could be made including stochastic foams, consolidated powders, honeycombs and lattice blocks or miniature truss structures. These structures can offer high performance features such as high strength accompanied by a relatively low mass, good energy absorption characteristics and good thermal and acoustic insulation properties, making them suitable for high value aerospace, medical and engineering products [63]. The concept of designed cellular materials is motivated by the desire to put material only where it is needed for a specific application, as nature does. Leonardo da Vinci stated: "In her (nature's) inventions, nothing is lacking, and nothing is superfluous". From a mechanical engineering viewpoint, a key advantage offered by cellular materials is high strength accompanied by a relatively low mass.

In the past 15 years, the area of lattice materials has received considerable research attention due to their inherent advantages over foams in providing light, stiff, and strong materials. Many methods have been developed to analyze various cellular structures. Wang and McDowell have performed a comprehensive review of analytical modeling, mechanics, and characteristics of various metal honeycombs [64,65]. Deshpande et al. [66] have investigated extensively lattice cells, particularly the octet-truss structure.

However, the cellular lattice structures proposed and investigated in the previous studies could not exhibit good manufacturability in SLM. As reported in a recent study, the cellular structures with large unit cell sizes (greater than 5 mm) could not be built using the SLM process because overhanging struts in the cells led to the occurrence of serious deformation [67]. This adds considerable constraints on manufacturing versatile and complex cellular structures to meet requirements of different functions and applications, sacrificing the design freedom of cellular structures and geometrical capability of AM manufacturing. Sacrificial support structures might be used to support overhanging structures and thus prevent deformation. On the counter side, support structures inside complex cellular lattice structures are normally not acceptable because they are very difficult to remove, and waste materials and energy.

It was demonstrated, by the authors chapter, that it is possible to manufacture aluminium lattice structures by DMLS as the ones reported in Figure 14, with desired shape and internal features in a single fabrication step. This was possible because previously many experiments were focused on investigating the limitations of building surfaces without support structures. An overhanging structure is a part of a component that is not supported during building, by solidified material or a substrate on the bottom side. Consequently, the melt pool created by the heat input from the laser is supported by powder material. From this definition, it is clear that a part of a component is an overhanging structure depending on the orientation given to the part while building it.
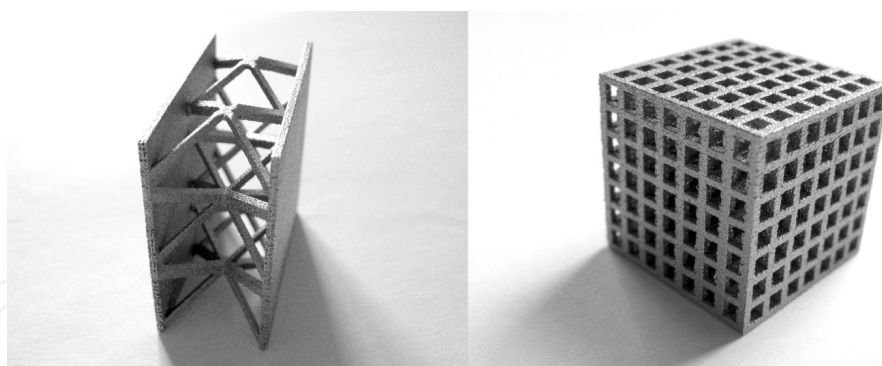
Figure 14. Lightweight components fabricated through DMLS in AlSiMg alloy.

In particular the cubic lattice structure of figure 14 was constructed with an angle of 45 degrees with respect to the building platform.

Following these design rules, a wide variety of different architectures can be made with fine control at the so called "cell level", as shown in Figure 15. The geometrical features selected for investigations were chosen because they could be the building blocks of more complex geometries. The structures have very good base metal properties thanks to the very fine microstructure typical of this process.
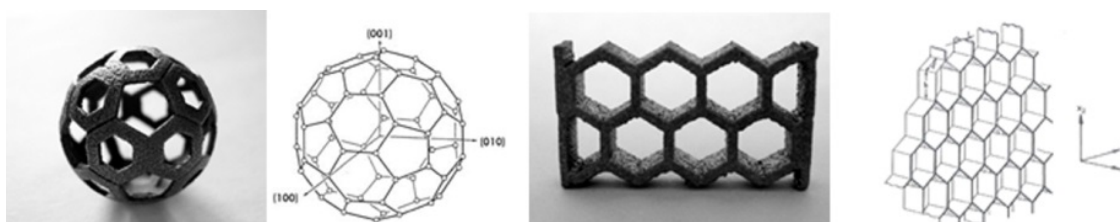

Figure 15. Cellular structures fabricated through DMLS in AlSiMg alloy: a fullerene structure (on the left), and a honeycomb cell structure (on the right).

8. Case study — Aluminium Matrix Composites (AMCs) by DMLS

As described in the previous paragraphs, aluminium alloys are currently produced by DMLS, in particular with compositions suitable for casting. The microstructure of these alloys is peculiar, since the very fast cooling occurring after the melting induced by laser provides an ultra-fine microstructure [34] and this effect is responsible for the significant increase of the mechanical properties that is observed with respect to conventional casting processes [37]. In fact, the conventional casting can be followed by a hardening heat treatment to improve its mechanical properties, treatment that seems not necessary in the case of DMLS process. Moreover, as a powder based process, DMLS also provides great opportunity to consolidate second or multiple material particles with metal powders to form novel metal matrix composites (MMCs). There is a growing research to develop MMCs via SLM process [68,69].

In order to be used inside a powder bed system, discontinuous ceramic particles are generally used. Among the most common reinforcement, silicon carbide (SiC) or aluminium oxide (Al_2O_3) are the most used, and in particular SiC-based AMCs are now widely used in many fields: from brake drums and cylinders liners of automobiles, to structural aerospace parts such as rotor vanes and plates. There are several methods to fabricate such composites: powder metallurgy, squeeze casting, stir casting or modified casting; however these conventional techniques are generally not suitable for complex shapes.

In the recent past different research groups investigated the feasibility to employ DMLS to obtain Al-based MMCs. Size and volume fraction of SiC particles have been varied to analyze the behavior of the composite [70], demonstrating that cracking occurs during the preparation by DMLS of these composites. In particular, crack density increases significantly after 15 volume percentage (vol.%) of SiC, and that there was not improvement of wear resistance over 20 vol.% of reinforcement. The same authors, in a previous study, found that microhardness increases with increase of volume fraction of SiC particles, as expected [39]. A couple of years before, Simchi et al. investigated the direct laser sintering of Al–7Si–0.3Mg/SiC composites [71], and showed that the densification rate increases at low SiC fractions but abruptly decreases at >~5 vol.%. Meanwhile, significant reaction occurs between the aluminium melt and the reinforcement particles, leading to formation of Al_4SiC_4 and silicon particles. However, these studies do not investigate the effects of process parameters on the density of metal matrix composites built by DMLS but the influence of design choices like supports generation and part orientation in the building chamber to avoid the presence of cracks during manufacture.

Starting from AlSiMg alloy, the possibility of composites fabrication by DMLS was investigated. The AlSiMg alloy has a high fluidity in the liquid phase, so that it is possible to prepare almost dense samples. Moreover, if silicon carbide is used a second phase, it is known in literature [72] that a high amount of silicon reduces or suppresses the reaction between aluminium and silicon carbide that brings to the formation of the dangerous aluminium carbide Al_4C_3, generally heavily detrimental for the mechanical properties. For this reason SiC particles were chosen as one of the possible reinforcing materials. α-SiC powders from H.C. Starck (UF-15, 15 m^2/g) were used, with density of 3.2 g/cm^3 and a mean particle size of 0.55 μm.

Another interesting reinforcement that was tested is the aluminium-magnesium spinel ($MgAl_2O_4$). This oxide has a high melting point of 2315 °C, a high Young's modulus and strength, and low thermal expansion coefficient (CTE). Moreover it is suggested in the literature [73] that it can improve substantially the creep behavior of composites if the size of the particles is very small. Thus nano-sized powders of $MgAl_2O_4$ were used (Nanocerox, mean size around 30 nm)

Since SiC particles are large while $MgAl_2O_4$ particles are much smaller, a different amount of the two reinforcements was used for the two composites, namely 10% and 1% in weight of SiC and $MgAl_2O_4$ respectively. To avoid deformation of the alloy spherical particles, simple mixing was done to prepare the composite powders, by using a ball milling system in ceramic jars, without any grinding medium, for 48 hours. The powders were then sieved with a mesh of 63 μm before putting them in the DMLS machine. The parameters used for the preparation of the composites are shown in Table 10.
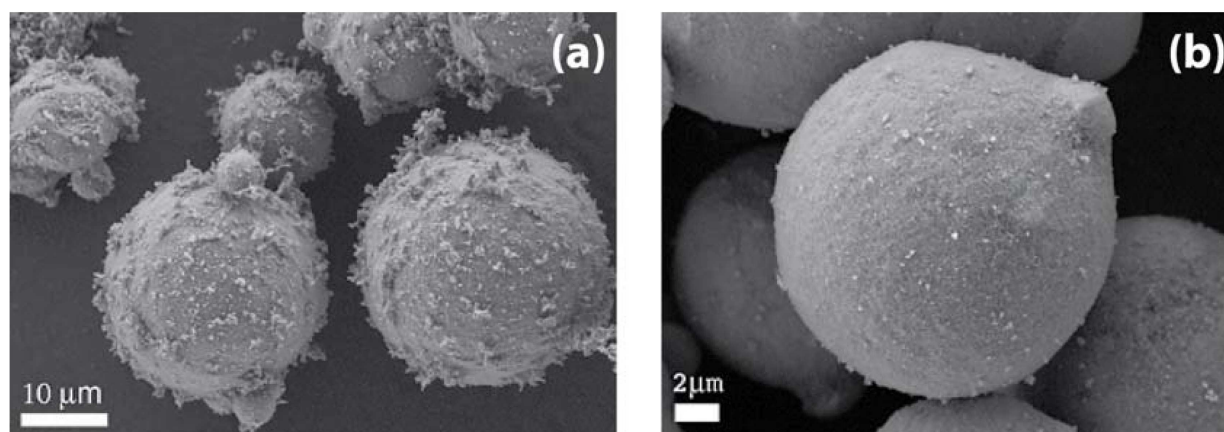
Figure 16. FESEM images of the composites powders: AlSiMg (a) and SiC (10%wt.) and (b) nano-MgAl$_2$O$_4$ (1%wt).

Parameters	AlSiMg	
	+ SiC	**+ MgAl$_2$O$_4$**
Scan speed (mm/s	500,700	600, 800
Laser Power (W)	180,195	195
Hatching dist. (mm)	0.17	0.17, 0.10

Table 10. Details of the process parameters employed.

In Figure 16 are shown the composite powders observed by FESEM. The metallic powders are not modified during the mixing process, however it is evident that both silicon carbide and nanospinel particles adhere on the surface of the aluminium alloy particles, and no agglomerates of pure ceramic particles are observed. In the case of silicon carbide the particles form a "fluffy" layer (Figure 16a), that causes an increased interaction between the surfaces of the powders. Thus, they have a different behavior in terms of flowability, causing some problems during the spreading of the powders, in particular in the first layers. This phenomenon is evident with silicon carbide, while it does not occur with the nanospinel (Figure 16b), probably due to the very small ceramic grain size and to the lower ceramic content. However it can be seen that the MgAl$_2$O$_4$ particles cover uniformly the round surface.

In the case of AlSiMg/SiC 10% composites, after a first step of parameter optimization, rectangular samples of 50x10x4 mm dimensions were obtained, with geometrical density between 2.59 and 2.61 g/cm^3. Since the theoretical density of these materials is 2.73 g/cm^3, the corresponding residual porosities are from 4.4 to 5%, a result in line with previous studies [39].

In the case of AlSiMg/SiC 10% composites, after a first step of parameter optimization, rectangular samples of 50x10x4 mm dimensions were obtained, with geometrical density between 2.59 and 2.61 g/cm^3. Since the theoretical density of these materials is 2.73 g/cm^3, the corresponding residual porosities are from 4.4 to 5%, a result in line with previous studies [39]. A problem however arises however with these composites: XRD measurements demonstrate

that silicon carbide is almost completely disappeared, while aluminium carbide is formed. This behavior is rather different to what happens for more conventional processes, where 10% Si is sufficient to suppress the Al-SiC reaction [72]. In this case, even if the contact time between molten alloy and ceramic is very low, the temperature is probably very high (in excess of 2000 K) and the reaction occurs. Ghosh et al. [39] already observed this phenomenon, but with a very low silicon content, while in the case of AlSiMg alloy the behavior was somewhat unexpected. The microstructure of the obtained composites is illustrated in the micrograph of Figure 17: it is very fine, as typical of the DMLS process, with elongated acicular grains, probably of Al_4C_3 as suggested by XRD analysis.
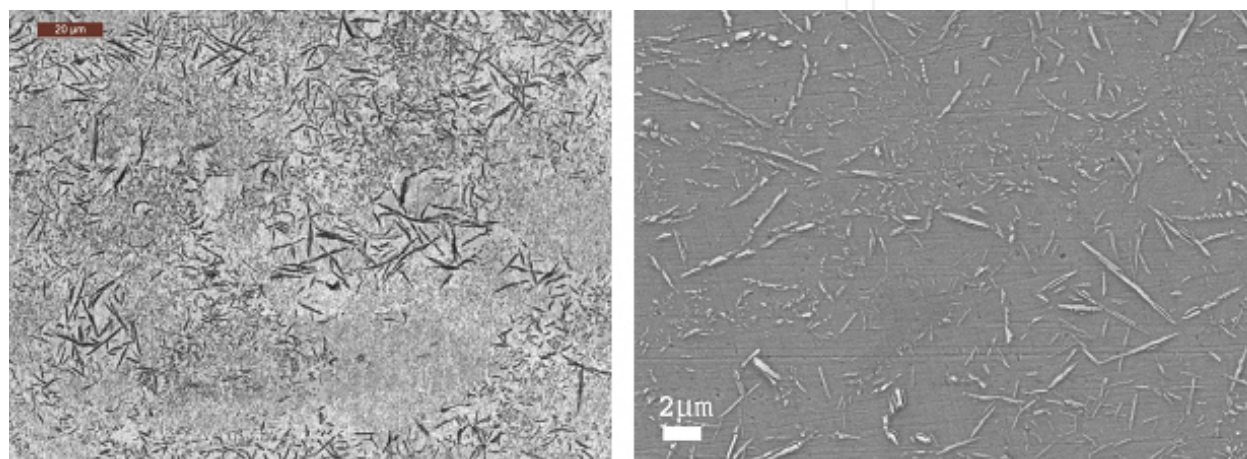

Figure 17. Optical (on the left) and FESEM (on the right) images of AlSiMg/SiC composite microstructure after polishing.

Residual SiC, instead, could be detected only in the very rare cases where some agglomerate is present, suggesting that the well dispersed single silicon carbide particle is instead completely reacted with the matrix. The presence of the ceramic reinforcement on hardness is in any case very evident: Brinell measurements mean value is 178 ± 2 HB for the SiC containing composites, which is 70% higher with respect to pure AlSiMg by DMLS.

In the case of nano-$MgAl_2O_4$ AMCs, the density is more depending on the specific choice of parameters than in the case of silicon carbide containing composites. In this case small samples were obtained to perform a more detailed screening of the parameters, and for this reason samples with 15x15x10 mm size were fabricated. With the parameters optimized in the best range, the measured average densities of the samples varied between 2.59 and 2.63 g/cm^3, corresponding to residual porosities in the range from 2.2 to 3.5% (the theoretical density is 2.689 g/cm^3).

In this case, the XRD analysis shows the presence of Al, Si, with some extremely small peaks that were attributed to the inter-metallic phase Mg_2Si and to some mixed metal-oxide of unknown origin (AlSiO$_x$), with a spectrum that is rather similar to the one of the pure alloy. Indeed, in this case the XRD technique is clearly less powerful to recognize possible reactions, due to the low content of reinforcing ceramic. The microstructure of these composites is also very similar to the case of the pure aluminium matrix, as illustrated in the micrographs of
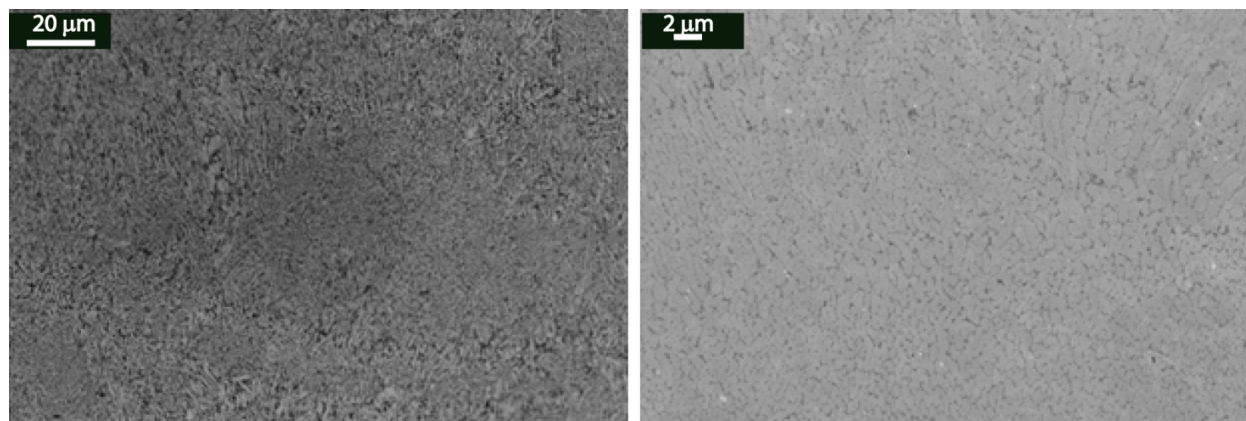
Figure 18. Optical (on the left) and FESEM (on the right) images of AlSiMg/Mg-nanospinel composite microstructures.

Figure 18. As typical of the DMLS process the microstructure is very fine, made by submicrometric grains, elongated in the correspondence of the melt pools contour due to the heat transfer flux direction. A careful observation however shows a higher inhomogeneity of these composites with respect to the pure aluminium alloy, suggesting that the presence of nano-$MgAl_2O_4$ particles changes the behavior during solidification. This inhomogeneity, together with the higher residual porosity, reflects on the values of Brinell Hardness, that is 93 ± 3 HB, 11% lower than the pure AlSiMg alloy processed through DMLS.

Acknowledgements

Author details

Diego Manfredi[1], Flaviana Calignano[1], Manickavasagam Krishnan[1,3], Riccardo Canali[1,2], Elisa Paola Ambrosio[1], Sara Biamino[2], Daniele Ugues[2], Matteo Pavese[2] and Paolo Fino[1,2]

1 Center for Space Human Robotics @Polito, Istituto Italiano di Tecnologia, Corso Trento, Torino, Italy

2 DISAT-Dipartimento Scienza Applicata e Tecnologia, Politecnico di Torino, Corso Duca degli Abruzzi, Torino, Italy

3 DIGEP – Dipartimento di Ingegneria Gestionale e della Produzione, Politecnico di Torino, Corso Duca degli Abruzzi, Torino, Italy

References

[1] Gibson I, Rosen WD, Stucker B. Additive Manufacturing Technologies-Rapid Proto-typing to Direct Digital Manufacturing. Springer; 2010.

[2] Wohlers T. Wohlers Report 2011 State of the Industry, Annual Worldwide Progress Report. Wohlers Associates; 2011.

[3] Campbell I, Bourell D, Gibson I. Additive manufacturing: Rapid prototyping comes of age. Rapid Prototyping Journal 2012; 18 (4): 255–258.

[4] http://www.amaze-project.eu/

[5] http://www.rapolac.eu/

[6] Gerrits A, Jones CL & Valero R. Custom-Fit: Quality of Life of European Sporting Public through Custom-Fit Products. The Engineering of Sport. 2006, 6: 5-10.

[7] http://www.e-break.eu/

[8] http://www.tialcharger.de/

[9] Wohlers T. Additive Manufacturing Advances. Manuf. Eng. 2012; 148 (4): 55–63

[10] Hot-Fire Tests Show 3-D Printed Rocket Parts Rival Traditionally Manufactured Parts. 2013. [Online]. Available: http://www.nasa.gov/exploration/systems/sls/3dprinting.html [Accessed: 13-Aug-2013].

[11] ASTM F2792-12a: Standard Terminology for Additive Manufacturing Technologies. DOI:10.1520/F2792-12A

[12] Calignano F, Manfredi D, Ambrosio EP, Iuliano L, Fino P. Influence of process parameters on surface roughness of aluminium parts produced by DMLS. Int. J. Adv. Manuf. Technol. 2013; 67 (9–12): 2743–2751.

[13] Aumund-Kopp C, Petzoldt F. Laser Sintering of parts with complex internal structures. In: Proceedings of the 2008 world congress on powder metallurgy & particulate materials. 2008; 1 (3): 385–397.

[14] Tsopanos S, Mines RAV, McKown S, Shen Y, Cantwell WJ, Brooks W, Sutcliffe CJ. The Influence of Processing Parameters on the Mechanical Properties of Selectively Laser Melted Stainless Steel Microlattice Structures. J. Manuf. Sci. Eng. 2010; 132 (4): 041011.

[15] Childs THC, Hauser C, Badrossamay M. Selective laser sintering (melting) of stainless and tool steel powders: experiments and modelling. Proc. Inst. Mech. Eng. Part B J. Eng. Manuf. 2005; 219 (4): 339–357.

[16] Tolosa I, Garciandía F, Zubiri F, Zapirain F, Esnaola A. Study of mechanical properties of AISI 316 stainless steel processed by 'selective laser melting', following different manufacturing strategies. Int. J. Adv. Manuf. Technol. 2010; 51 (5–8): 639–647.

[17] Li R, Liu J, Shi Y, Du M, Xie Z. 316L stainless steel with gradient porosity fabricated by selective laser melting. J. Mater. Eng. Perform. 2010; 19 (5): 666–671.

[18] Averyanova M, Cicala E, Bertrand P, Grevey D. Experimental design approach to optimize selective laser melting of martensitic 17-4 PH powder: part I – single laser tracks and first layer. Rapid Prototyping Journal. 2012; 18 (1): 28–37.

[19] Dewidar MM, Dalgarno KW, Wright CS. Processing conditions and mechanical properties of high-speed steel parts fabricated using direct selective laser sintering. Proc. Inst. Mech. Eng. Part B J. Eng. Manuf. 2003; 217 (12): 1651–1663.

[20] Yasa E, Deckers J, Kruth JP, Rombouts M, Luyten J. Charpy impact testing of metallic selective laser melting parts. Virtual Phys. Prototyp. 2010; 5 (2): 89–98.

[21] Li X, Wang C, Zhang W, Li Y. Fabrication and compressive properties of Ti6Al4V implant with honeycomb-like structure for biomedical applications. Rapid Prototyping Journal. 2010; 16 (1): 44–49.

[22] Vrancken B, Thijs L, Kruth JP, Van Humbeeck J. Heat treatment of Ti6Al4V produced by Selective Laser Melting: Microstructure and mechanical properties. J. Alloys Compd. 2012; 541: 177–185.

[23] Van Hooreweder B, Moens D, Boonen R, Kruth JP, Sas P. Analysis of Fracture Toughness and Crack Propagation of Ti6Al4V Produced by Selective Laser Melting. Adv. Eng. Mater. 2012; 14 (1–2): 92–97.

[24] Song B, Dong S, Zhang B, Liao H, Coddet C. Effects of processing parameters on microstructure and mechanical property of selective laser melted Ti6Al4V. Mater. Des. 2012; 35: 120–125.

[25] Marcu T, Todea M, Gligor I, Berce P, Popa C. Effect of surface conditioning on the flowability of Ti6Al7Nb powder for selective laser melting applications. Appl. Surf. Sci. 2012; 258 (7): 3276–3282.

[26] Wang Z, Guan K, Gao M, Li X, Chen X, Zeng X. The microstructure and mechanical properties of deposited-IN718 by selective laser melting. J. Alloys Compd. 2012; 513: 518–523.

[27] Yadroitsev I, Pavlov M, Bertrand P, Smurov I. Mechanical properties of samples fabricated by selective laser melting. In: 14èmes Assises Européennes du Prototypage & Fabrication Rapide, 2009.

[28] Kumar S, Pityana S. Laser-based additive manufacturing of metals. Adv. Mater. Res. 2011; 227: 92–95.

[29] Kumar S. Selective Laser Sintering: Recent Advances. In: 4th Pacific International Conference on Applications of Lasers and Optics. Wuhan-China, 2010.

[30] Khan M, Dickens PM. Processing parameters for Selective Laser Melting (SLM) of gold. In: Proceedings of Solid Freeform Fabrication symposium, 2008: 278–289.

[31] Louvis E, Fox P, Sutcliffe CJ. Selective laser melting of aluminium components. J. Mater. Process. Technol. 2011; 211 (2): 275–284.

[32] Olakanmi EO, Dalgarno KW, Cochrane RF. Laser sintering of blended Al-Si powders. Rapid Prototyping Journal. 2012; 18 (2): 109–119.

[33] Olakanmi EO, Cochrane RF, Dalgarno KW. Densification mechanism and microstructural evolution in selective laser sintering of Al – 12Si powders. J. Mater. Process. Technol. 2011; 211 (1): 113–121.

[34] Thijs L, Kempen K, Kruth JP, Van Humbeeck J. Fine-structured aluminium products with controllable texture by selective laser melting of pre-alloyed AlSi10Mg powder. Acta Mater. 2013; 61 (5): 1809–1819.

[35] Kempen K, Thijs L, Yasa E, Badrosamay M, Verheecke W, Kruth JP. Process optimization and microstructural analysis for selective laser melting of AlSi10Mg. In: Proceedings of Solid Freeform Fabrication symposium, 2011: 484–495.

[36] Manfredi D, Calignano F, Ambrosio EP, Krishnan M, Canali R, Biamino S, Pavese M, Atzeni E, Iuliano L, Fino P and Badini C. Direct Metal Laser Sintering: an additive manufacturing technology ready to produce lightweight structural parts for robotic applications. La Metallurgia Italiana. 2013; 105 (10): 15-24.

[37] Manfredi D, Calignano F, Krishnan M, Canali R, Ambrosio EP, Atzeni E. From Powders to Dense Metal Parts: Characterization of a Commercial AlSiMg Alloy Processed through Direct Metal Laser Sintering. Materials. 2013; 6 (3): 856-869.

[38] Kumar S, Kruth JP. Composites by rapid prototyping technology. Mater. Des. 2010; 31 (2): 850–856.

[39] Ghosh SK, Saha P, Kishore S. Influence of size and volume fraction of SiC particulates on properties of ex situ reinforced Al-4.5Cu-3Mg metal matrix composite prepared by direct metal laser sintering process. Mater. Sci. Eng. A, 2010; 527 (18–19): 4694–4701.

[40] Thijs L, Verhaeghe F, Craeghs T, Humbeeck JV, Kruth JP. A study of the microstructural evolution during selective laser melting of Ti-6Al-4V. Acta Mater. 2010; 58 (9): 3303–3312.

[41] Spierings AB, Herres N, Levy G. Influence of the particle size distribution on surface quality and mechanical properties in AM steel parts. Rapid Prototyping Journal. 2011; 17 (3): 195–202.

[42] Buchbinder D, Schleifenbaum H, Heidrich S, Meiners W, Bültmann J. High Power Selective Laser Melting (HP SLM) of Aluminum Parts. Phys. Procedia 2011; 12: 271–278.

[43] Qiu C, Adkins NJE, Attallah MM. Microstructure and tensile properties of selectively laser-melted and of HIPed laser-melted Ti-6Al-4V. Mater. Sci. Eng. A, 2013; 578: 230–239.

[44] Thijs L, Montero Sistiaga ML, Wauthle R, Xie Q, Kruth JP, Van Humbeeck J. Strong morphological and crystallographic texture and resulting yield strength anisotropy in selective laser melted tantalum. Acta Mater., 2013; 61 (12): 4657–4668.

[45] Kruth JP, Badrosamay M, Yasa E, Deckers J, Thijs L, Van Humbeeck J. Part and material properties in selective laser melting of metals. In: Proceedings of the 16th International Symposium on Electromachining (ISEM XVI), 2010.

[46] Shiomil M, Yamashital T, Osakada K, Shiomi M, Yamashita T, Abe F, Nakamura K. Residual Stress within Metallic Model Made by Selective Laser Melting Process. Ann. CIRP, 2014; 53 (1): 195–198.

[47] Zaeh MF, Branner G. Investigations on residual stresses and deformations in selective laser melting. Prod. Eng., 2009; 4 (1): 35–45.

[48] Kruth JP, Yasa E, Deckers J. Roughness improvement in Selective Laser Melting. In: Proceedings of the 3rd International Conference on Polymers and Moulds Innovations. PMI, 2008: 170–183.

[49] ASM Handbook, Volume 2-Properties and Selection: Non ferrous Alloys and Special-Purpose Materials, and Volume 4 – Heat treating. 1990, ASM International The Materials Information Company, United States of America, ISBN 0-87170-379-3.

[50] Hauser C, Childs THC, Badrossamay M. Further developments in process mapping and modelling in direct metal selective laser melting. In: Proceedings of the Solid Freeform Fabrication symposium, 2004; 448–459

[51] Krishnan M. Investigation of material and mechanical properties of Al alloy and Al based MMC parts produced by DMLS for industrial application. PhD Thesis. Politecnico di Torino; 2014.

[52] Hertzberg RW. Deformation and Fracture Mechanics of Engineering Materials. John Wiley & Sons Inc, 1996.

[53] Brandl E, Heckenberger U, Holzinger V, Buchbinder D. Additive manufactured Al-Si10Mg samples using Selective Laser Melting (SLM) Microstructure, high cycle fatigue, and fracture behavior. Materials and Design. 2012; 34: 159-169.

[54] Delgado J, Ciurana J, Rodríguez CA. Influence of process parameters on part quality and mechanical properties for DMLS and SLM with iron-based materials. Int J Adv Manuf Technol. 2012; 60:601–610

[55] Kruth JP, Levy G, Klocke F, Childs THC. Consolidation phenomena in laser and powder-bed based layered manufacturing. CIRP 2007; 56(2):730–759

[56] Dalgarno K. Materials research to support high performance RM parts. Rapid Manufacturing 2nd International Conference, Loughborough University, 2007; 147–56

[57] Sachdeva A, Singh S, Sharma VS. Investigating surface roughness of parts produced by SLS process. Int J Adv Manuf Technol. 2012.

[58] Evans A, Bruno G. Relaxation of residual stress in shot peened Udimet 720Li under high temperature isothermal fatigue. Int J Fatigue. 2005; 27: 1530–1534.

[59] Turski M, Clitheroe S, Evans AD, Rodopoulos C. Engineering the residual stress state and microstructure of stainless steel with mechanical surface treatments. Appl Phys A. 2010; 99: 549–56.

[60] Murr LE, Gaytan SM, Ramirez DA, Martinez E, Hernandez J, Amato KN, Shindo PW, Medina FR, Wicker RB. Metal Fabrication by Additive Manufacturing Using Laser and Electron Beam Melting Technologies. J. Mater. Science Technology. 2012; 28(1): 1–14.

[61] Ashby MF et al., Metals Foams: A Design Guide. Woburn, MA: Butterworth-Heinemann, 2000.

[62] Gibson LJ, Ashby MF. Cellular Solids, Structure and Properties. 2nd Edition, Cambridge University Press, Cambridge, 1997.

[63] Williams CB, Cochran JK, Rosen DW. Additive manufacturing of metallic cellular materials via three-dimensional printing. Int. J. Adv. Manuf. Technol. 2011; 53: 231–239.

[64] Wang AJ, McDowell DL, Optimization of a metal honeycomb sandwich beam-bar subjected to torsion and bending. Int. J. Solids Struct. 2002; 40(9): 2085-2099.

[65] Wang AJ, McDowell DL. Yield surfaces of various periodic metal honeycombs at intermediate relative density. Int. J. Plasticity. 2005; 21(2): 285-320.

[66] Deshpande VS, Fleck NA, Ashby MF. Effective properties of the octet-truss lattice material. Journal of Mechanics and Physics of Solids. 2001; 49(8): 1747-1769.

[67] Yan C, Hao L, Hussein A, Raymont D. Evaluations of cellular lattice structures manufactured using selective laser melting. International Journal of Machine Tools & Manufacture. 2012; 62: 32–38.

[68] Kumar S, Kruth JP. Composites by rapid prototyping technology. Materials and Design. 2010; 31: 850-856.

[69] Hao L, Dadbakhsh S. Materials and process aspects of selective laser melting of metals and metal matrix composites: a review. Chinese Journal of Lasers. 2009; 36 (12): 3192–3203.

[70] Ghosh SK, Saha P. Crack and wear behavior of SiC particulate reinforced aluminium based metal matrix composite fabricated by direct metal laser sintering process. Materials and Design. 2011; 32: 139-145.

[71] Simchi A, Godlinski D. Effect of SiC particles on the laser sintering of Al–7Si–0.3Mg alloy. Scripta Materialia. 2008; 59: 199-202.

[72] Narciso J, García-Cordovilla C, Louis E. Reactivity of thermally oxidized and unoxidized SiC particulates with aluminium-silicon alloys. Materials Science and Engineering B. 1992; 15: 148-155

[73] De Vita A, Roitti S, Sbaizero O. Creep of aluminium metal matrix composites reinforced with magnesium spinel. Key Engineering Materials. 2004; 264-268: 953-956.